Structural mass reduction by integrating active material in direct drive generator design

J. N. Stander, G. Venter & M. J. Kamper

Structural and Multidisciplinary Optimization

ISSN 1615-147X

Struct Multidisc Optim
DOI 10.1007/s00158-015-1243-y

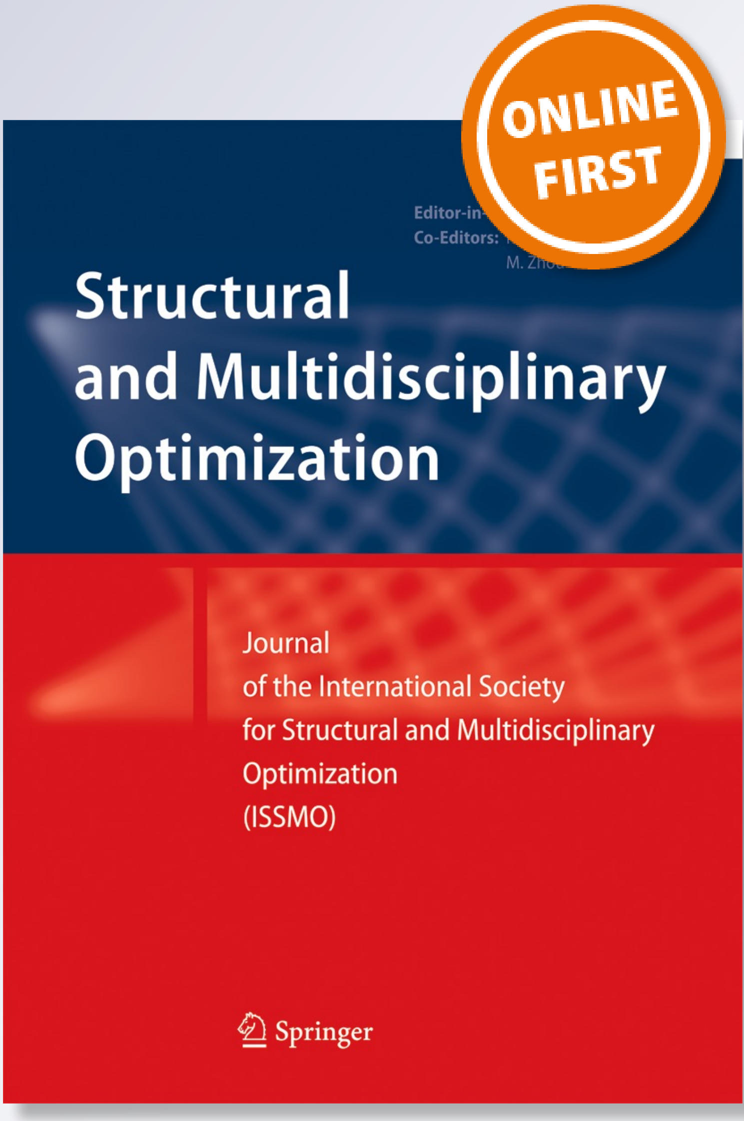

Struct Multidisc Optim
DOI 10.1007/s00158-015-1243-y

INDUSTRIAL APPLICATION

Structural mass reduction by integrating active material in direct drive generator design

J. N. Stander[1] · G. Venter[1] · M. J. Kamper[2]

Received: 17 November 2014 / Revised: 24 February 2015 / Accepted: 10 March 2015

Abstract Permanent magnet synchronous generator technology is known for its low power to mass ratio. Its heavy structural design results from the need to ensure a small air-gap at a large diameter between stator and rotor parts. Numerous options for lowering structural mass are considered. In this paper, an overall mass reduction strategy which entails the integration of the magnetically active parts with the support structure are presented. Two three megawatt generator designs, one with a single bearing and the other with double bearing lay-up, are considered. These models comprise three-dimensional elements, isotropic and orthotropic materials, linear static extreme hub loads, and magnetic stresses. Shape and size optimisations are applied in calculation of structural mass saving incurred from structural integration and the altering of rotor and stator yoke thicknesses. The results show that total generator mass reduction is possible through the integration of the active material.

Keywords Sizing · Shape optimisation · Structural · Generator · Wind turbine

✉ J. N. Stander
jstander@sun.ac.za

G. Venter
gventer@sun.ac.za

M. J. Kamper
kamper@sun.ac.za

1 Department of Mechanical and Mechatronic Engineering, University of Stellenbosch, Private Bag X1, Matieland, 7602, Stellenbosch, South Africa

2 Department of Electrical and Electronic Engineering, University of Stellenbosch, Private Bag X1, Matieland, 7602, Stellenbosch, South Africa

1 Introduction

The wind turbine industry has migrated from an era of utilisation to one of drive-train diversification, especially in the large multi-megawatt class. The highly efficient permanent magnet (PM) direct drive generator drive-trains account for about 11 % of the 2012 global wind turbine market share (Krogsgaard et al. 2013). Such a low market share may be ascribed to the heavy structural design, dependency on expensive rare earth materials, the cost and size limitations on mechanical bearings, and the highly customised manufacturing processes.

The heavy rotor and stator structures arise from the high structural stiffness targets that are governed by high magnetic stresses, large air-gap diameters, and air-gap deflections constraints (i.e. 10 %) (Polinder et al. 2013; je Bang et al. 2008). The radial air-gap dimension is typically $0.001D_\delta$, where D_δ is the mean air-gap diameter which varies between 3 and 6 m. The electro-magnetic stresses are closely related to the air-gap dimension. The nature of this relation depends on the rigidity of the hub-generator coupling or interface. Air-gap deflections are caused by extreme hub loads, construction irregularities, operational faults, etc. Bearing material is the most expensive structural material in a generator design. The arrangement and bore size of the mechanical bearing also affect the generator cost per mass

Published online: 26 April 2015

balance. For example, a single suspension bearing design has less structural material but consists of an expensive large bore bearing (moment bearing) (SKF 2014). The structural design of direct drive PM generators are highly customised. Manufacturers use different materials and apply various stiffening schemes. Their designs also differs in the type

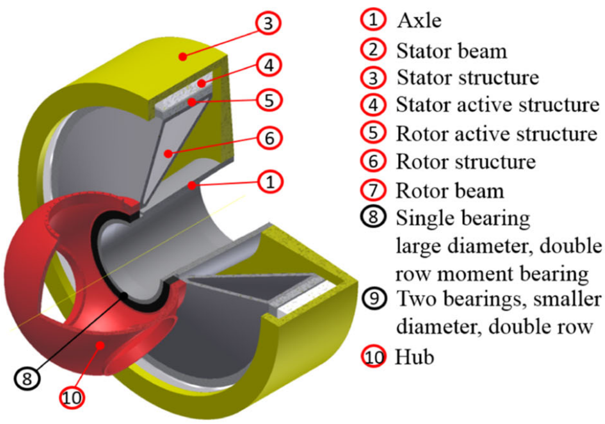

(a) Model SB (Single Bearing)

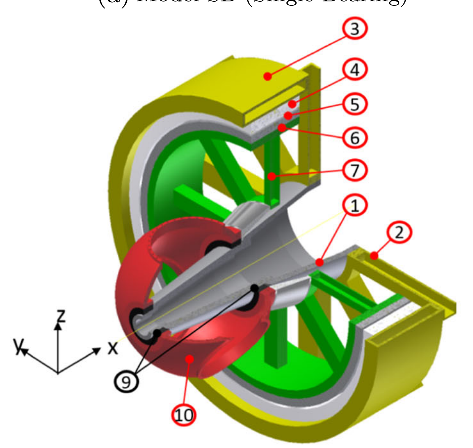

(b) Model DB (Double Bearing)

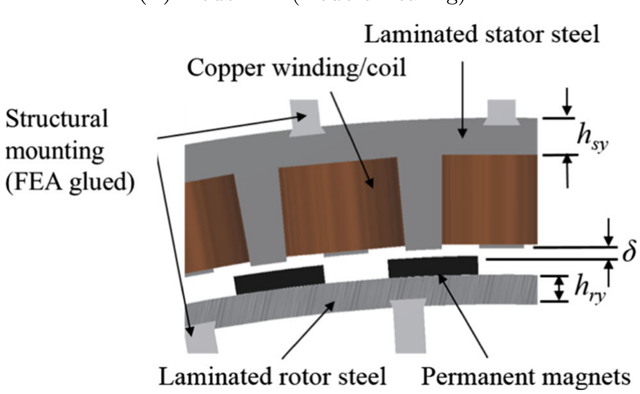

(c) Electro-magnetic components where h_{sy}, h_{ry}, δ are the stator yoke height, rotor yoke height, and air-gap height, respectively

Fig. 1 The generator models and the electro-magnetic assembly of conventional designs

and number of ancillary equipment (e.g. braking system and heat exchangers), and sub-assemblies. schemes explored in research and industry involve:

- replacing rotor shaft with rotor axle (Stander et al. 2012),
- minimising the amount of large diameter mechanical bearings (Versteegh 2004),
- changing a double bearing configuration to a single bearing configuration with the addition of numerous smaller bearings at the air-gap (i.e NewGen concept) (Engström et al. 2004),
- increasing the wind turbine hub-generator structural integration (Versteegh 2004),
- changing the generator topology from internal rotor to external rotor,
- changing the generator magnetic flux orientation and active design (i.e. C-Gen concept) (Keysan et al. 2010; Zavvos et al. 2012),
- introducing structural flexibility through the utilisation of active support systems like active magnetic bearings (Shrestha et al. 2010),
- the use of lighter materials such as aluminium and GFRE (Stander et al. 2012).

A reduction in overall generator mass is possible by integrating the available electro-magnetic active steel with the structural design. This approach may require minimal modification to an existing electro-magnetic design. The cost implication is negligible, based on the small difference between active and structural steel specific costs (McDonald et al. 2008). In this paper, the results of such a mass minimisation study are presented, involving two electrically similar three megawatt direct drive generator models, of which only the structural mass is minimised through shape and size optimisation, including specific rotor and stator yoke size alterations. Dynamic and stochastic hub loads following fatigue life concerns were not considered. Subsequently, the two direct drive generator models are discussed, followed by an explanation of the model simplifications and the finite element modelling procedure. The latter concerns the materials, as well as the loads, and elements that are applied. Lastly, the shape and size optimisation setup are stipulated and the results are discussed.

2 Modelling

2.1 Physical models

The generator models that are considered, consist of an axle, a hub, mechanical bearings, a PM rotor assembly and a stator assembly. Both models are separately driven by a 125 m turbine rotor. The hub is rigidly fixed to the PM rotor assembly (Fig. 1a to c). The models are distinguished by bearing support, i.e. Model SB is the single bearing design and Model DB has the double bearing layout.

The SB model is configured with an external PM rotor that encapsulates the stator, e.g. VENSYS design. Altogether, such a configuration yields an even lighter and more compact generator. However, this configuration was not considered in this study. Model SB comprises a large bore ($\geq$ 2 m) spherical roller bearing that is located between a hollow axle and the PM rotor assembly. The bearing is placed near the hub-rotor interface. The structural design of the PM rotor may be described as a torus with a triangular cross section. The stator structure consists of a thin-wall cylinder, stiffened at both ends by disks. Model DB has two double-row spherical roller bearings of different bore diameters. Structurally, the PM rotor comprises eight rectangular beams and a solid thin-wall cylinder. These beams are equally spaced around the rotating axis (x-axis in Fig. 1b). The stator structure consists of a torus with a rectangular cross section, which in turn is supported with eight rectangular beams. These beams are rigidly fixed to the stator and the axle.

The electro-magnetic design of these models is identical. Machine dimensions were calculated using a lumped analytic model as described by Stander et al. (2014). It's a radial flux synchronous design fitted with a non-overlapping copper winding (Germishuizen and Kamper 2010). This winding is coupled to a grid via a power electronic converter which alters (i.e. lowering) the electrical frequency of the machine in order to maximise power. The machine is excited with PMs which in turn are glued/welded to the rotor stack. The low machine frequency allows for the PMs to be directly mounted to the rotor support structure. However, such a design is not considered here. The large air-gap diameter practically limits the stator and rotor laminate dimensions hence each laminate is divided in to smaller sections. In this study the stator and rotor stacks are divided into 16 equal sections along the air-gap circumference. Structurally, similar hub-PM rotor and stator-turret interfaces are assumed. The axle does not transfer all hub loads; instead, the rigid hub-PM rotor coupling creates a secondary load path.

Wind turbine hub and electro-magnetic induced loads are transferred to the wind turbine tower at the generator-turret coupling. The electromagnetic induced loads mentioned here refer to the generator counter-torque and the magnetic pull caused by rotor eccentricity. An unbalanced magnetic pull between stator and rotor yields a bending moment at the generator-turret interface. The bearing placements relative to the hub and the PM rotor interfaces will affect the air-gap deformations; however, the details are beyond the scope of this paper. The general design specifics of the two models are listed in Table 1.

2.2 Finite element models

All finite element models (FEMs) were generated using the *MSC Nastran* version 2012 code. The simplifications applied in the modelling are as follow:

- hub loads are transferred to the axle via rigid body element type 3 (RBE 3)
- bearings are represented using RBE type 2 elements (see Section 2.3)
- the PM rotor torque is restricted to the rated value
- the effects of thermal stresses are neglected
- the axle wall thickness is constant along its length
- the laminated steel cores (i.e. yokes) are modelled as 3-D solid elements with orthotropic material properties (Pirnat et al. 2013)
- the stiffening added by the impregnated stator winding and glued magnets are neglected

Figure 2a and b shows the FEM models setup for shape and size optimisation. Note, that for both models all six degrees of freedom (d.o.f.) are constrained at the turret side. Both Model SB and Model DB consist of electro-magnetic active and designable structural parts. These designable parts are modelled as a combination of solid, shell and beam elements which have isotropic (MAT1) material properties. A detailed description of the applied elements types and the limitations thereof are documented in Lampert and McLean (2011). The complex and detailed geometries of the laminated stator and rotor steel stacks are reduced to simple sector sections (Section 2.1). Each sector section is viewed as a single solid part with orthotropic properties (Pirnat et al. 2013) in a cylinderical reference frame. Linear contact (touch) boundary conditions are assigned to the circumferential interface between any two adjacent sections. Each section is glued (see Fig. 1c) to the its support structure. In this study, the winding (coils), stator teeth and PMs are not modelled as structural load carrying parts. The specific masses of the latter parts are included as 0-D concentrated mass elements (CONM2) allocated to circumferential nodes facing the air-gap. The yokes are modelled having orthotropic material properties in a cylinderical sense with moduli: E_r = 205 kN/mm^2, E_t = 205 kN/mm^2, and E_z = 185 kN/mm^2.

The stator and rotor beams of Model DB are presented using simple 2-D beam elements. The stator support structure is represented as thin wall cylinders and disks comprising linear shell elements (QUAD4). Most support structures of Model SB are modelled with QUAD4 elements. The

Table 1 Design specifications

Parameters	Values [SI units]
Wind turbine	
wind class [IEC]	III_A
rated wind speed [m/s]	7.0
rotor operation	Variable speed
rated rotor rotation speed [rpm]	11
air density [kg/m^3]	1.225
Rotor design	
number of blades	3.
nominal rotor diameter [m]	125.
nominal rotor mass [kg] (hub inc.)	70 000.
axle material (cast iron)	EN-GJS-700
Hub layout	
hub diameter[m]	2.6
axial length [m]	2.85
center of mass [m]	0.75
Generator	
rated power [kW]	3000.0
mechanical air-gap [mm]	5.0
stack axial length [m]	1.0
stack material	M400-65A
stator and rotor yoke height [mm]	25.0
slot height [mm]	80.0
magnet height [mm]	12.0
rotor stack mass [kg]	2 857.0
stator stack mass [kg]	8 715.0
magnet mass [kg]	1 010.0
copper mass [kg]	3 704.0
rotor and stator materials	steel grade 1040

bearing pressures and displacements exerted on the axle and PM rotor are indirectly calculated, see Section 2.3). Designing the wind turbine hub was beyond the scope of this study, therefore a rigid hub design was assumed. The hub representation consists of an array of RBE 3 elements that have a common centre node. The applied hub loads are defined at the central node. Unlike RBE 2 elements, the RBE 3 elements are not rigid and only interpolate and distribute loads and displacements.

Mesh dependency studies of the above FE models were performed. Mesh convergence measure is the maximum radial air-gap deformation. These deformations are plotted against the number of shell and solid elements, see Fig. 2c. The number of elements selected for Model SB and Model DB are 40560 and 197040, respectively.

2.3 Bearing modelling

Detailed FE modelling of bearings incorporate non-linear material properties and contact models which in turn require fine detailed meshes. In this study such detail is not required hence substituting models are sought. In literature (Chunjun 2009; Ghalamchi et al. 2013; Golbach 1999), bearing FE models include simplified raceway geometries and substituting roller models. Rollers are represented using beam, spring or bush elements (Molnár et al. 2012). The number and arrangement of these elements are governed by roller type and topologies. The bearing assemblies in Models SB and DB are subjected to extreme hub loads. Such loads may result in the bearings being the stiffest structural components. Therefore, following a conservative approach, bearings were modelled as arrays of 1-D RBE 2 elements. This approach presents the worst case scenario in terms of hub load induced air-gap displacements. The stiffness of the RBE 2 and the elastic bush (Molnár et al. 2012) bearing models were indirectly compared by calculating the maximum radial outer raceway deformation $d\gamma$ specific to the bearing in Model SB. The maximum radial deformations calculated for the bush and RBE 2 bearing models are $-1.375 \cdot 10^{-3}$ m and $-3.396 \cdot 10^{-6}$ m, respectively. The latter is the stiffest bearing model hence large air-gap deformations are expected.

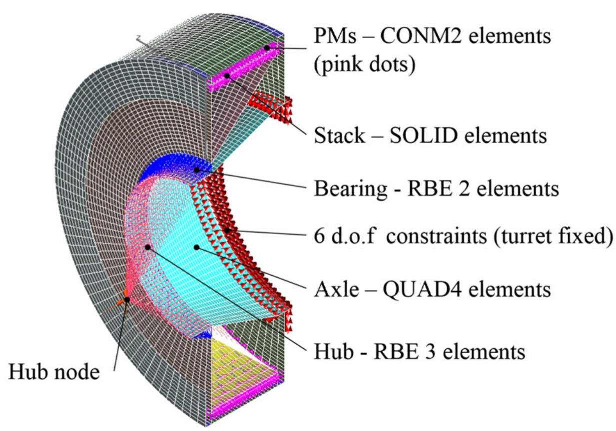

(a) Model SB

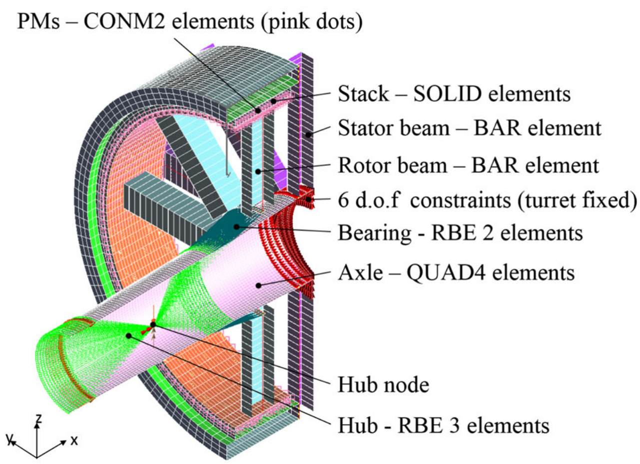

(b) Model DB

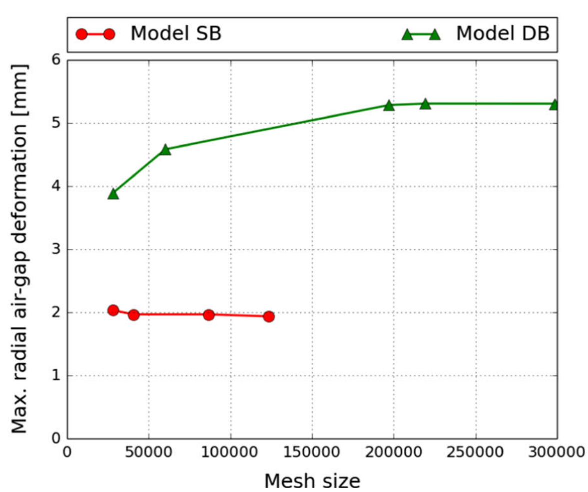

(c) Model mesh convergence results

Fig. 2 Finite element model setups and checks

3 Loads

Specific to a generator, the loads acting on a machine are either induced by a wind turbine rotor (external) or by the electro-magnetic excitation source (internal). External loads are hub loads and gravitational loads whereas, internal loads are thermally and magnetically induced loads. Dynamic control induced and vibrational loads are also present, but are not considered. The applied hub and electro-magnetic loads considered are of a quasi-static nature. External loads affect internal loads; for example the closing of the generator air-gap caused by extreme hub bending moments

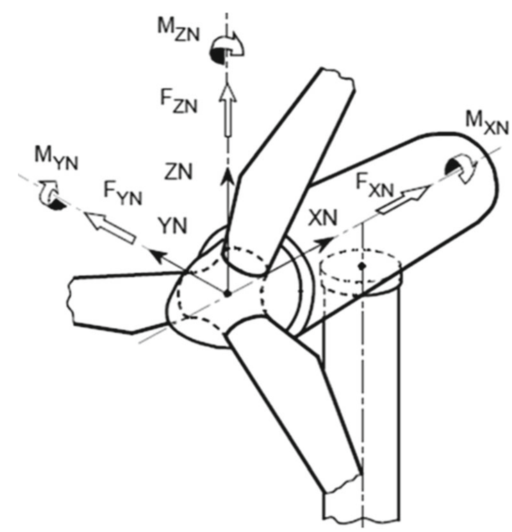

Loads	
F_{Xmax} [kN]	963.
F_{Ymax} [kN]	452.
F_{Zmax} [kN]	-1 390.
M_{Xmax} [kN·m]	3 956.
M_{Ymax} [kN·m]	10 020.
M_{Zmax} [kN·m]	9 578.

Fig. 3 Extreme hub loads in the stationary hub coordinate system (Germanischer 2010)

will yield an altered magnetic flux distribution, i.e. electro-magnetic stresses. The electro-magnetic stress sensitivity to external loads depends on the level of generator structural integration. The two models considered have high levels of generator structural integration hence, hub loads were taken into consideration. The following sections present the calculation of loads specific to the design specifications listed in Table 1.

3.1 Global loads

The global loads are inertial forces caused by gravitational and centrifugal accelerations. Two gravitational forces are considered: the first acts along the axial direction (e.g. transportation), and the other acts along the vertical axis (e.g. operation phase). Bearing and hub masses are neglected in both cases. The gravitational acceleration applied is 9.81 m/s^2. The PM rotor centrifugal force is calculated for a constant rotational speed of 11 rpm.

3.2 Hub loads

The calculated hub loads incorporate the extreme wind and turbulence models specific to a class III$_{\mathrm{A}}$ wind regime. These models are detailed in the 2010 wind turbine design certification guidelines by Germanischer (2010). Load variations induced by the wind turbine pitch, generator and yaw power control schemes, grid connection, and converter operation are ignored. Only the extreme hub load values derived from the complex aerodynamic loading produced by the 125 m wind turbine rotor are considered. These were estimated using a multi-body linearised wind turbine design code *Bladed v8.25*. Extreme hub loads are derived from a combination of load cases, as described in Germanischer (2010). These loads are assigned to the hub node, as depicted in Fig. 2a and b. The hub load values are tabulated in Fig. 3. Note that the applied rotor torque is not an extreme hub load, but is derived from the rated magnetic stresses calculated in Section 3.3.

3.3 Electro-magnetic loads

The air-gap (Fig. 1c) between PM rotor and stator is uniform so that uniformly distributed electro-magnetic stresses are generated. The peak tangential and normal stresses are calculated using Maxwell equations represented in (1) and (2), respectively (Pyrhönen et al. 2009),

$$\tau = \frac{1}{2}\hat{B}_n \hat{A} \cos\delta_t \tag{1}$$

$$\sigma_n = \frac{\hat{B}_n^2}{2\mu_0} \tag{2}$$

where $\hat{B}_n$ and $\hat{A}$ are the respective peak values of the normal flux density component and the electric loading. The related design values are given in Table 2. The angle δ_t is the torque angle and function $\cos\delta_t$ defines the internal power factor. In a PM excited machine, the peak flux density per pole pair is calculated in (3)

$$\hat{B}_n(k) = \frac{4h_m B_{rm}}{(1-\varepsilon)g_{eff}\,\mu_{rm}\nu\pi} sin\left(\frac{\nu\pi w_m}{2w_p}\right) \tag{3}$$

where B_{rm} is the remanent flux density, $\varepsilon = \frac{e}{g_{eff}}$ is the relative eccentricity, g_{eff} is the effective air-gap, h_m and w_m are the magnet height and pitch, w_p is the pole pitch, and ν the ν^{th} harmonic. The large air-gap allows for the omission of the armature reaction in the calculation of $\hat{B}_n$.

Table 2 The electro-magnetic design specifics

Symbol	Parameter	Value
f_n	machine frequency [Hz]	20.0
ν	ordinal of flux harmonic	1
$2p$	number of pole pairs	110.0
$\hat{B}_n$	peak air-gap flux density [T]	1.0
E_{ph}	stator phase voltage [V]	1 100.0
k_{fill}	slot fill factor	0.6
Q	number of slots	264.
e	eccentricity [mm]	1.7
g_{eff}	effective air-gap [mm]	17.0
D_δ	mean air-gap diameter [m]	4.75
$\hat{A}$	peak electric loading [kA/m]	85.0
δ_t	torque angle [°]	30.0
μ_0	vacuum permeability [H/m]	$4\pi \cdot 10^{-7}$

Eccentricity (Shrestha 2013), in the radial sense, caused by external loading or assembly defects, yields a cosine shaped magnetic stress distribution. Here the magnetic pull peaks where the air-gap clearance is the smallest. The effect of axial eccentricity is negligible. Magnetic stress variation in the axial sense is small in comparison to stress caused by aerodynamic load variation, i.e. changes in wind speed.

A rotor eccentricity of 10 %, assimilating generator manufacturing and assembly defects, is included in the magnetic stress calculations. The applied tangential and normal stresses calculated are about 40 kN/m^2 and 400 kN/m^2, respectively. These stresses are defined as normal and tangential pressures on the rotor outer, and stator inner circumferences, respectively.

4 Sizing and shape optimisation setup

The optimisation procedure is illustrated in Fig. 4 below. The mass minimisation shape and size optimisation problem is formulated in (4). Variables in (4) are explained in Section 4.2. The optimisation procedure is illustrated in Fig. 4.

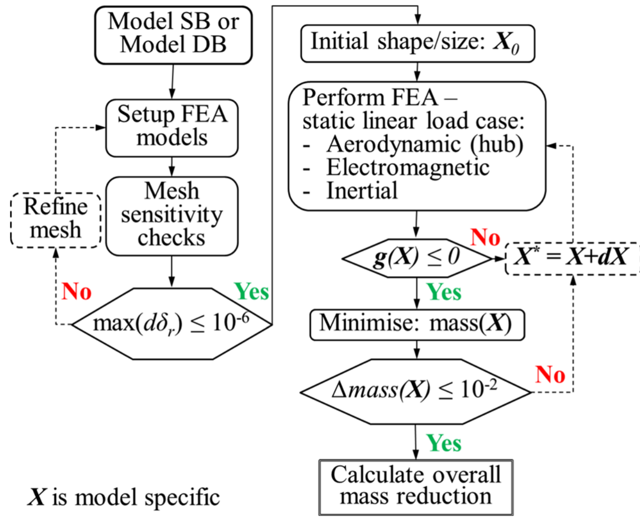

Fig. 4 Flow diagram of model optimisation procedure

Table 3 Declaration of variables in design vector **X**

Models	Variables	Range [m]
Model SB		
axle wall thickness	ax_t	0.01–0.25
rotor conical disk thickness	rdb_t	0.01–0.1
rotor cylinder thickness	rc_t	0.01–0.1
rotor disk thickness	rfd_t	0.01–0.1
stator back disk thickness	sbd_t	0.01–0.1
stator cylinder thickness	sc_t	0.01–0.1
stator front disk thickness	sfd_t	0.01–0.1
stator cylinder radius (shape)	sfd_r	2.0–2.5
Model DB		
axle wall thickness	ax_t	0.01–0.25
bearing cylinder thickness	b_t	0.01–0.05
rotor cylinder thickness	rc_t	0.01–0.1
stator cylinder thickness	sc_t	0.01–0.1
stator disk thickness	sd_t	0.01–0.1
stator top cylinder thickness	st_t	0.01–0.1
stator top radius (shape)	sr_r	2.5–2.75
rotor beam thickness 1	rb_{t1}	0.005–0.05
rotor beam thickness 2	rb_{t2}	0.005–0.05
rotor beam depth	rb_d	0.05–0.5
rotor beam width	rb_w	0.05–0.5
stator beam thickness 1	sb_{t1}	0.005–0.05
stator beam thickness 2	sb_{t2}	0.005–0.05
stator beam depth	sb_d	0.05–0.5
stator beam width	sb_w	0.05–0.5

Table 4 Baseline designs; active structures excluded

Models	Values [m]
Model SB	
axle wall thickness	0.1
rotor conical disk thickness	0.05
rotor cylinder thickness	0.05
rotor disk thickness	0.05
stator back disk thickness	0.05
stator cylinder thickness	0.05
stator front disk thickness	0.05
stator front disk radius	2.0
total structural mass [kg]	43 317.
Model DB	
axle wall thickness	0.1
bearing cylinder thickness	0.05
rotor cylinder thickness	0.05
stator cylinder thickness	0.05
stator disk thickness	0.05
stator top cylinder thickness	0.05
stator top radius	2.75
rotor beam thickness 1	0.02
rotor beam thickness 2	0.02
rotor beam depth	0.34
rotor beam width	0.40
stator beam thickness 1	0.02
stator beam thickness 2	0.02
stator beam depth	0.25
stator beam width	0.4
total structural mass [kg]	45 640.

Table 5 Masses of optimised structural designs in [kg]

Models	Structural	Active	Total
Model SB			
Case 1 (no active)	13 253.	16 286.	29 539.
Case 2 (yoke 0 %)	7 269.	16 286.	23 555.
Case 3 (yoke 25 %)	7 555.	18 555.	26 110.
Case 4 (yoke 50 %)	6 237.	19 925.	26 162.
Case 5 (yoke 100 %)	7 352.	23 327.	30 679.
Model DB			
Case 1 (no active)	29 416.	16 286.	45 702.
Case 2 (yoke 0 %)	21 130.	16 286.	37 416.
Case 3 (yoke 25 %)	20 381.	18 555.	38 936.
Case 4 (yoke 50 %)	19 822.	19 925.	39 747.
Case 5 (yoke 100 %)	19 440.	23 327.	42 767.

Table 6 PM rotor and stator structural masses in [kg]

Models	PM Rotor	Stator	Total
Model SB			
Case 2 (yoke 0 %)	3 388.	2 759.	6 097.
Case 3 (yoke 25 %)	3 152.	2 752.	5 905.
Case 4 (yoke 50 %)	2 407.	2 796.	5 204.
Case 5 (yoke 100 %)	1 633.	2 852.	4 485.
Model DB			
Case 2 (yoke 0 %)	5 954.	9 509.	15 463.
Case 3 (yoke 25 %)	5 257.	8 650.	13 908.
Case 4 (yoke 50 %)	4 709.	9 336.	14 045.
Case 5 (yoke 100 %)	3 806.	9 529.	13 335.

A commercial optimisation code, *Genesis v13.1* by VR&D (Vanderplaats 2014), was applied. The optimisation starts by initialising the design vectors of Model SB and Model DB, respectively. Each vector $\boldsymbol{X}$ comprises the geometric dimensions of the axle, the structural members (e.g. beam width), and the rotor and stator yokes. The static load case applied is a linear combination of the loads described in Section 3. Stresses and deformations are calculated using the embedded sparse matrix solver (Vanderplaats 2014). This is followed by the calculation and the verification of constraints. Then, if constraints are satisfied, $\boldsymbol{X}$ is either updated or altered such that the overall model mass is minimised. The optimisation loop is terminated when the change in model mass is less than 1 %.

$$
\begin{aligned}
&\underset{X}{\text{minimise}}\ \ \text{mass}(X)\\
&\text{subject to}\\
&g_1 = \vartheta_i(X) - 1.0 \le 0, \quad i = 1, \ldots, 16\\
&g_2 = 5.0 - |\lambda_1| \le 0\\
&g_3 = \sigma_{cast}(X)/480 \cdot 10^6 - 1.0 \le 0\\
&g_4 = \sigma_{steel}(X)/320 \cdot 10^6 - 1.0 \le 0\\
&g_5 = \sigma_{active}(X)/200 \cdot 10^6 - 1.0 \le 0
\end{aligned}
\tag{4}
$$

4.1 Design variables

Design vector $\boldsymbol{X}$ entries specified for each models are defined in Table 3. Note that the physical range of each variable is also specified. Baseline design values of Model SB and Model DB are given in Table 4. The thicknesses of shell elements are limited to approx. 15 % of the diameter rotor, stator, axle, etc. This ensures that the finite element model conforms to the Mindlin-Reissner plate theory (Oñate 2013).

4.2 Constraints

Referring to (4), five inequality design constraints are applied. The first constraint (g_1) limits the radial deformation of rotor and stator at the air-gap to 1.0 mm (20 % of air-gap clearance). This deformation limit strictly accommodates the described extreme hub loading condition, and as such it does not represent common operational design requirements (Section 1). This limit is applied to 16 nodes distributed around the air-gap circumferences of both the rotor and the stator. A buckling load factor constraint specific to the buckling first mode $|\lambda_1| > 5$ (Novoselac et al. 2012) is applied as a second constraint (g_2). The final three design constraints limit the maximum Von Mises stresses in the axle, in the structural members, and in the rotor and stator yokes. Here the denominators are the tensile strengths in N/mm^2.

4.3 Optimisation case studies

Five structural optimisation cases were considered. Each case entails both Model SB and Model DB. In Case 1 the

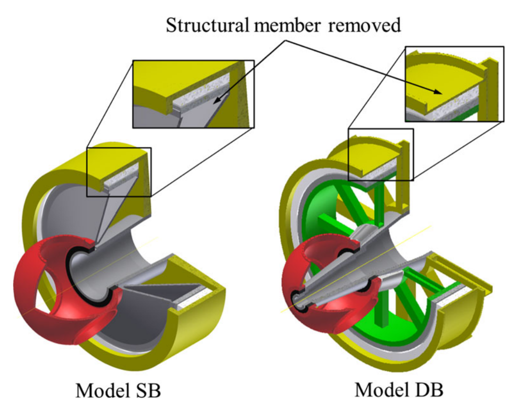

Fig. 5 Structural material removed in optimised designs with increased yoke dimensions

common generator design practise is followed where the active structure is excluded from the structural design. Case 2 involves the integration of the PM rotor and stator yokes. Cases 3 to 5 entail the structural integration of altered yokes. In Cases 3 to 5 the yoke thicknesses are radially increased by 25 %, 50 %, and 100 %, respectively.

5 Optimisation results

The size and shape optimisation results of Model SB and Model DB are shown in Table 5 where the structural masses (excluding bearings, bolts, etc.) calculated for five different structural integration cases are presented. In Case 1 all active structures are excluded from the FE models, hence no structural stiffening by active structures. Only the representative masses of the latter were included. The mass elements (CONM2s) are equally distributed around the air-gap circumferences of the PM rotor and stator.

The rest of the cases (Case 2 to 5) listed in Table 5 relate the structural integration of the PM rotor and stator yokes (see Section 2.2). A zero % yoke means that the radial yoke height is not increased from the initial 25 mm (Table 1). Whereas a 25 % yoke implies that the radial yoke height is increased by 25 %, i.e. yoke height equals 31.25 mm. The

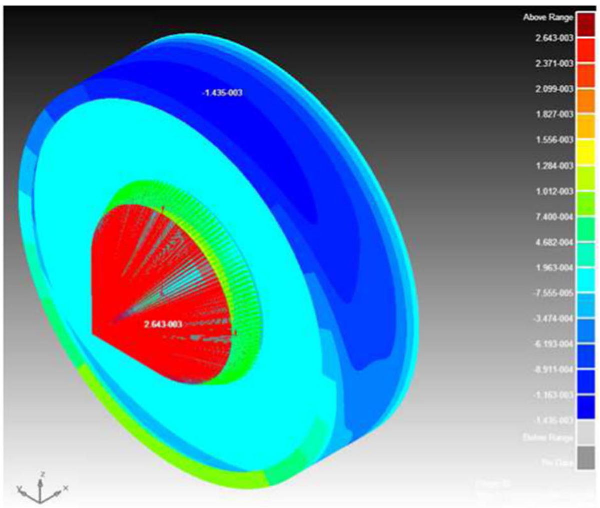

(a) Model SB displacements in (m); max. 0.002 m

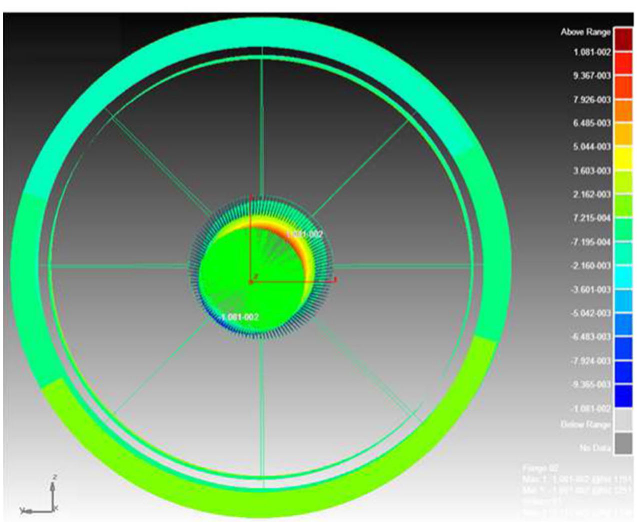

(b) Model DB displacements in (m); max. 0.01 m

Fig. 6 Finite element analysis deformation results: cylindrical reference frame for optimised designs with 25 % increase yoke heights

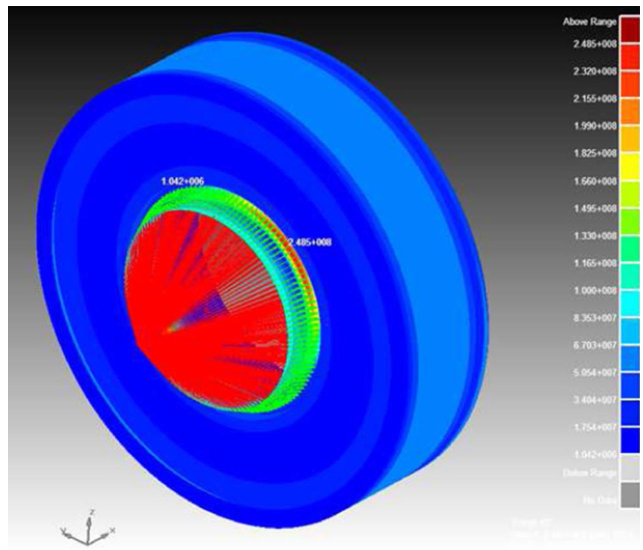

(a) Model SB stresses in (N/mm^2); max. 248 N/mm^2)

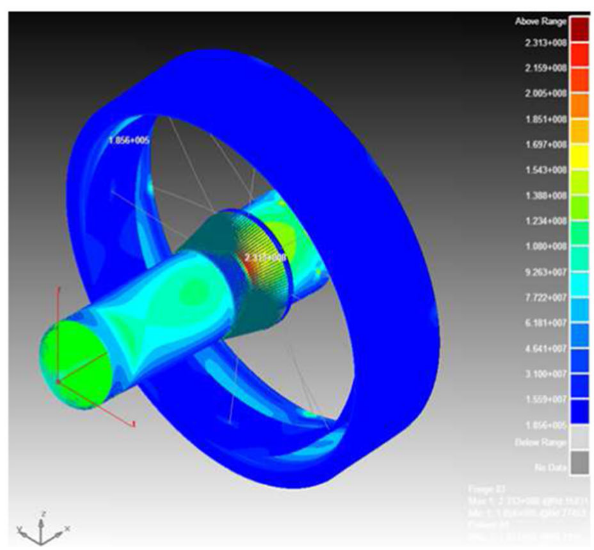

(b) Model DB stresses in (N/mm^2); max. 231 N/mm^2

Fig. 7 Finite element analysis Von Mises stress results: cylindrical reference frame for optimised designs with 25 % increase yoke heights

PM rotor and stator yoke dimensions are radially increased in the inward and outward directions, respectively. At first glance, the figures confirm that the structural integration of the active parts yields a reduction in the overall generator mass for both models. It is also clear that the overall generator mass is highest when the active structures are not included in the structural optimisation. These figures hint that the largest overall mass reduction can be significant when the yoke dimensions are kept as initially specified. The reduction amounts to 5 984 kg and 8 286 kg for Model SB and Model DB respectively. Wind turbine top mass reduction is beneficial because in lowers transportation and installation costs. Of the two models considered, Model SB is the lightest. Its large-bore hollow axle provides a very stiff support. However, this design requires a large bore bearing which is at least an order more expensive than both bearings used in the DB model. The breakdown of the PM rotor and stator support structure masses are given in Table 6. Note that these mass values do not included in the axle masses.

The most mass reduction is noted in the PM rotor structural design (Table 6). However, the mass reductions will affect the structural dynamics of these designs. To what extent, is yet to be analysed. This structural mass reduction is also more pronounced in Model SB. The structural need of some stiffening members are replaced by the altered yokes. Figure 5 indicates which structural members are redundant. These include part of the PM rotor cylinder and the external stator cylinder (Fig. 1a and b).

The air-gap deformation modes that have the greatest affect on the generator's performance, are localised rotor/stator radial warping and rotor eccentricity. The structural integration of active material may counter warping, whereas the stiffening of the axle, and the turbine rotor load separation may lessen the rotor eccentricity effects. Generator structural mass is sensitive to the localised stiffness of the annular air-gap structures. Thus, if most stiffening is required at the air-gap, more flexible rotor and stator structures may be possible. Stiffening of active parts may be possible by introducing stiffer electrical steels or by adding composite laminates between the electro-magnetic active laminates. Increased rotor and stator structural flexibility may be achieved by utilising, for example, a different support design (Engström et al. 2004), and active bearing supports (Shrestha 2013).

The finite element analysis results of the optimised models which 25 % increased yokes are indicated in Figs. 6 and 7. Large axle displacements are evident in the nodal displacement plots shown in Fig. 6a and b. Displacements near the bearing locations exceed the air-gap thickness of 5.0 mm. It is therefore clear that a design of the proposed direct-drive generator structures must include the axle design and hub loads, since these structurally affect the generator rotor. Rotor and stator structures can also be lighter by isolating the turbine torque from other hub loads, for example by incorporating the Alstom *Pure Torque* concept (Puigcorbe and de Beaumont 2010).

6 Conclusion

The integration of active material (stator and rotor stacks) as structural support, yields an overall mass reduction for the two single and double bearing generator designs considered. The increase of both the stator and rotor yoke thickness may also result in the replacement of some of the structural steel members. This option may cause no additional expenses, because the specific costs of active steel and structural steel (low carbon steel) are nearly similar. Simple linear static optimisation results have indicated that the largest overall mass reduction can be significant when the yoke dimensions are kept as initially specified. However, the optimal dimension is sensitive to the allowable air-gap deformation, the stiffness of the generator axle and active steels, the mechanical bearing selected, and the hub loads transferred to the rotor and stator structures.

Acknowledgments The author would like to thank the Development Bank of Southern Africa, which funded this research through its GreenFund initiative. The grant number is RW1/1035.

References

Chunjun P (2009) Static analysis of rolling bearings using finite element method. Master's thesis, *Baustatik und Baudynamik*. University of Stuttgart

Engström S, Hernnäs B, Parkegren C, Waernulf S (2004) Development of NewGen - A new type of direct-drive generator. In: Proceedings of european wind energy conference and exhibition. London, EWEA, pp 1–10

Germanischer (2010) Germanischer Lloyd - guideline for the certification of wind turbines, Hamburg. http://www.gl-group.com

Germishuizen JJ, Kamper MJ (2010) Classification of symmetrical non-overlapping three-phase windings. 2010 XIX International Conference on Electrical Machines (ICEM) pp 1–6. doi:10.1109/ICELMACH.2010.5608096

Ghalamchi B, Sopanen J, Mikkola A (2013) Simple and versatile dynamic model of spherical roller bearing. Int J Rotating Mach 2013(567542):1–13. doi:10.1155/2013/567542

Golbach H (1999) Integrated non-linear fe module for rolling bearing analysis. In: Proceedings of NAFEMS WORLD CONGRESS 99 on Effective Engineering Analysis, National agency for finite element methods and standards, vol 2. NAFEMS, Rhode Island

je Bang D, Polinder H, Shrestha G, Ferreira J (2008) Promising direct-drive generator system for large wind turbines. In: Wind power to the grid - EPE wind energy chapter 1st seminar. doi:10.1109/EPEWECS.2008.4497321

Keysan O, McDonald A, Mueller M, Doherty R, Hamilton M (2010) C-GEN, A lightweight direct drive generator for marine energy converters. In: 5th IET International conference on power electronics, machines and drives (PEMD 2010), pp 1–6 doi:10.1049/cp.2010.0021

Krogsgaard P, Madsen BT, Zhao F, Karcanias A, Hamilton B (2013) A BTM Wind Report-World Market Update 2012 - International Wind Energy Development - Forecast 2013–2017, 1st edn. Navigant Consulting

Lampert L, McLean DM (2011) MSC NASTRAN - Linear static analysis user's guide, vol 2012. MSC.Software Corporation

McDonald AS, Mueller MA, Polinder H (2008) Structural mass in direct-drive permanent magnet electrical generators. Renew Power Gener, IET 2(1):3–15. doi:10.1049/iet-rpg:20070071

Molnár L, Váradi K, Bódai G, Zwierczyk P, Oroszváry L (2012) Simplified modelling for needle roller bearings to analyse engineering structures by fem. Period Polytech - Mech Eng 54(1):27–33. doi:10.3311/pp.me.2010-1.05

Novoselac S, Ergić T, Baliċević P (2012) Linear and nonlinear buckling and post buckling analysis of a bar with the influence of imperfections. Tehniċki Vjesnik 19(3):695–701

Oñate E (2013) Structural analysis with the finite element method - linear statics, Springer Netherlands

Pirnat M, Čepon G, Boltežar M (2013) Introduction of the linear contact model in the dynamic model of laminated structure dynamics: an experimental and numerical identification. Mechanism and Machine Theory 64:144–154

Polinder H, Ferreira J, Jensen B, Abrahamsen A, Atallah K, McMahon R (2013) Trends in wind turbine generator systems. IEEE J Emerg Sel Top Power Electron 1(3):174–185. doi:10.1109/JESTPE.2013.2280428

Puigcorbe J, de Beaumont A (2010) Wind turbine gearbox reliability: the impact of rotor support. Renewable Energy World Magazine. http://www.renewableenergyworld.com, online; accessed August 2013

Pyrhönen J, Jokinen T, Hrabovcová V (2009) Design of rotating electrical machines. Wiley

Shrestha G (2013) Structural flexibility of large direct drive generators for wind turbines. PhD dissertation, Technical University Delft, Delft

Shrestha G, Polinder H, Bang DJ, Ferreira JA (2010) Structural flexibility: A solution for weight reduction of large direct-drive wind-turbine generators. IEEE Trans Energy Convers 25(3):732–740. doi:10.1109/TEC.2010.2048713

SKF (2014) SKF Nautilus. online, http://www.skf.com/.../skf-nautilus.html

Stander JN, Venter G, Kamper MJ (2012) Review of direct-drive radial flux wind turbine generator mechanical design. Wind Energy 15(3):459–472. doi:10.1002/we.484

Stander JN, Kamper MJ, Venter G (2014) Analytic modelling and optimization of slip synchronous permanent magnet wind turbine generator topologies. Wind Energy. doi:10.1002/we.1756

Vanderplaats (2014) Vanderplaats Research and Development - Genesis. http://www.vrand.com/genesis.html

Versteegh CJA (2004) Design of the Zephyros Z72 wind turbine with emphasis on the direct drive PM generator. Trondheim. http://www.elkraft.ntnu.no/norpie/info.html

Zavvos A, McDonald AS, Mueller M, Bang DJ, Polinder H (2012) Structural comparison of permanent magnet direct drive generator topologies for 5 MW wind turbines. In: 6th IET International Conference on Power Electronics, Machines and Drives (PEMD 2012), pp 1–6. doi:10.1049/cp.2012.0286